Spectrochimica Acta Part A: Molecular and Biomolecular Spectroscopy 268 (2022) 120681

Contents lists available at ScienceDirect

Spectrochimica Acta Part A: Molecular and Biomolecular Spectroscopy

journal homepage: www.elsevier.com/locate/saa

Facile one-step fabrication of Cu-doped carbon dots as a dual-selective biosensor for detection of pyrophosphate ions and measurement of pH

Ying Yang [1], Chaofeng Wang [1], Qin Shu, Na Xu, Shuangqing Qi, Shujuan Zhuo, Changqing Zhu, Jinyan Du *

Anhui Key Laboratory of Chemo-Biosensing, Key Laboratory of Functional Molecular Solids, Ministry of Education, College of Chemistry and Materials Science, Anhui Normal University, Wuhu 241000, PR China

HIGHLIGHTS

- The Cu-CDs with a dual-selective feature were successfully fabricated through a one-step hydrothermal carbonization.
- The Cu-CDs can be served as a highly selective and sensitive fluorescent probe for the detection of PPi, where the detection limit was estimated to be 0.013 μM.
- Due to a pH-dependent fluorescence emission feature and visual color change, the Cu-CDs can be applied to pH sensing and pH-paper for urine.

GRAPHICAL ABSTRACT

The fluorescent Cu-CDs were served as a dual-selective nanosensor to detect PPi based on fluorescence enhancing with linearity from 0.05 to 20 μM and LOD of 0.013 μM, and pH value by observing color with naked eye under UV lamp through an assembled portable paper-based sensor of pH.

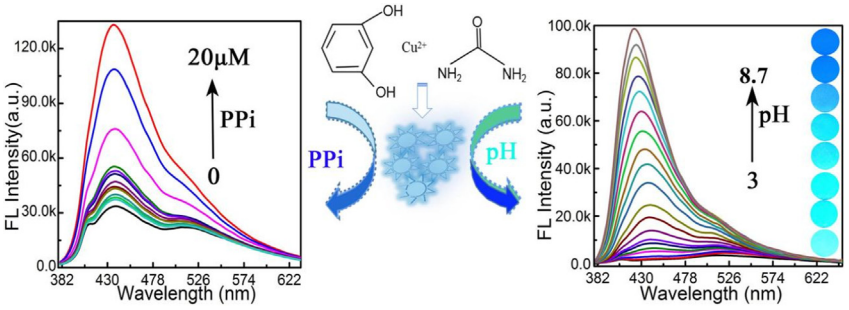

ARTICLE INFO

Article history:
Received 25 August 2021
Received in revised form 19 November 2021
Accepted 26 November 2021
Available online 30 November 2021

ABSTRACT

High-performance determination of pyrophosphate ions (PPi) and pH is an important goal in biological systems. In this work, Cu-doped carbon dots (Cu-CDs) were synthesized rapidly and simply via a one-pot hydrothermal method. The as-obtained Cu-CDs, with an average size of 2.55 nm, exhibit an excitation-independent fluorescence emission and possess desirable functional groups of carboxyl and amine, which can be served as fluorescence nanoprobes for detection of PPi based on surface passivation. Under the optimal condition, the linear range for detection of PPi was 0.05–20 μM, and the corresponding limit of detection (LOD) was 0.013 μM, indicative of a promising assay for the PPi. Moreover, the fluorescent intensity of the Cu-CDs is linear against pH value from 6 to 8.7 in buffer solution, suggesting the feasibility as a pH sensor. The synthesized Cu-CDs coated fluorescent paper indeed can monitor pH in urine with satisfaction by naked eyes through ultraviolet irradiation. The successful detection of PPi and the visual detection of pH value suggest a highly promising application of Cu-CDs in the field of biosensing.

1. Introduction

Anions and pH are of vital importance in both biological and natural systems [1,2]. As a by-product of DNA replication and a hydrolyzed product of adenosine triphosphate in living cells [3,4], the anion of pyrophosphate ($P_2O_7^{4-}$, PPi) exists elsewhere in the biological environments. However, excessive or low PPi concentration in biological systems would lead to a variety of diseases, including chondro-calcification, calcium pyrophosphate deposition disease (CPPD), and rheumatism [5–7]. To monitor or diagnose these diseases, the detection of PPi concentrations in biological environments is urgently needed [8,9]. Moreover, a high dosage

* Corresponding author.
E-mail address: dujinyn@mail.ahnu.edu.cn (J. Du).
[1] Ying Yang and Chaofeng Wang contributed equally to this work.

https://doi.org/10.1016/j.saa.2021.120681
1386-1425/

of PPi has been reported as one of the main factors for water eutrophication, and high concentrations of PPi in rivers and soil, in turn, lead to high doses in humans [10]. Therefore, it is highly desirable to develop a sensitive chemical sensor for the detection of PPi.

On the other hand, measurement of pH is ubiquitous in many areas, such as water quality testing [11], environmental monitoring [12], clinical measurements (e.g., blood and urine) [13], and food safety inspection [14]. In particular, intracellular pH plays a vital role in various physiological and pathological processes [15], such as apoptosis, cell cycle, ion transport, receptor-mediated signal transduction, inflammation, tumor growth, and muscle contraction [16], as it modulates the structure and function of all biologically active macromolecules. Moreover, small changes in pH in body fluids, e.g., urine, would represent the changes in the internal environment of the body. Furthermore, the pH of urine can reflect the acid-base balance in the body and the regulation function of the kidney. Therefore, a parameter with paramount importance for proper biological function and hence for measurement in all of the experimental biosciences is the proton concentration, i.e., the pH [17,18]. Nowadays, most of the pH measurements are made with glass pH probes, which generally suffer from some inconvenience, e.g., frequent recalibration, difficulty in miniaturization, wet storage of the glass membrane, and interferences from alkali metals [19,20]. Additionally, the glass pH probes are delicate and require careful handling, making it difficult for in-situ analyses. Hence, it remains unremitting pursuit to develop a simple, flexible, and sensitive pH sensor [21–24].

As a novel type of zero-dimensional carbon nanomaterial, carbon dots (CDs) not only present tunable optical properties but also exhibit outstanding characteristics including bright fluorescence, water-solubility, excellent photo-stability, nontoxicity, anti-photobleaching chemical stability, as well as fascinating biocompatibility [25–27]. Due to the excellent optical properties, CDs have shown enormous application prospects in photocatalysis, chemical and biological sensing, bioimaging, photodynamic therapy, and drug delivery [28,29]. To date, several CDs-based sensors have been developed for the detection of PPi, in which the CDs were used as either reference or response signals [30–32]. Particularly, in the majority of these sensing strategies, metals (M^{Z+}: Fe, Cu, Pb, Ni, Co, etc.) are generally required to play an important role as a bridge during the detection process. For examples, Yu et al. prepared the blue emission N-CDs via the hydrothermal method from ammonium citrate to detect the Fe^{3+} and PPi by "on-off-on" strategy [33]. Dai and co-workers prepared the S, N, O-CDs from m-phenylenediamine and sulfamide by using the hydrothermal method for detecting Cu^{2+} and PPi via the strong interaction between Cu^{2+} and PPi [34]. Jiang and co-workers designed the bright-blue fluorescent CDs with sodium citrate and polyacrylamide for the determination of Pb^{2+} and PPi [35]. Yue and colleagues proposed a blue emission of CDs that can be remarkably quenched by Cu^{2+}, Ni^{2+}, Mn^{2+}, and Co^{2+} due to the coordination reaction between metal ions and the carboxylic groups on the surface of CDs, and the recovery of CDs triggered by PPi realized the quantitative detection of PPi [31]. In truth, most of the PPi-specific fluorescence CDs sensing mechanism was believed as the competitive coordination effects between M^{Z+} - CDs interaction and M^{Z+} - PPi interaction. Although some reported fluorescent CDs have excellent performance for sensing PPi, undoubtedly, these PPi detection strategies are slightly complicated. Therefore, the direct, rapid, and one-step detection and monitoring of PPi, is urgently needed.

Meanwhile, many pH fluorescent CDs probes have also been developed. Wang's group synthesized the dual-emission CDs as a probe for the determinations of pH [36]. Nie et al. prepared two types of CDs from chloroform ($CHCl_3$) and diethylamine (DEA) for pH sensing with a good linearity in the range of pH from 5 to 8 [37]. Liu et al. reported the dual-emissive N, S-CDs, which presented a distinct pH-sensitive feature with a good linear relationship between the fluorescence intensity of CDs and pH values [38]. Huang's groups developed the red fluorescence carbon dots (RCDs) platform for the testing of environmental samples such as cattle urine and lake water with good results [39]. In this sense, the development of a dual-selective nanosensor that simultaneously realizes the detection of PPi and pH for biological system-related indicators is still of important concern.

With this thought in the mind, herein, we designed a dual-emission Cu-doped carbon dots (Cu-CDs), being synthesized by a simple, one-step hydrothermal method, which can be used for a rapid and direct detection of PPi and sensing of pH (Scheme 1). Specifically, it not only can directly detect PPi quickly and sensitively, but also can visually measure the pH value by observing color with the naked eyes under UV lamp through an assembled portable paper-based sensor of pH, which was prepared by simple coating the Cu-CDs on the commercial filter paper. It is worth noting that the color change range is relatively associated with the pH of urine samples, and the corresponding color change can be also achieved in actual urine samples, which would open up a considerable practical prospect for the direct, rapid and sensitive detection of pH for body fluids. As a consequence, the unique feature with detection of two targets would enable this new sensor broad application in biosensing in the future.

2. Experimental section

2.1. Reagents and materials

All the Chemical agents used were of analytic grade. Resorcinol, urea (UR), $CuSO_4$, pyrophosphate, 2-[4-(2-Hydroxyethyl)-1-piperazinyl] ethane sulfonic acid (HEPES) and dialysis membrane (MWCO of 1000 Da) were purchased from Aladdin Chemistry Co. Ltd. (Shanghai, China). A Milli-Q plus 185 equipped from Millipore (Bedford, MA) was employed to purify the water. All glass wares were washed with aqua regia (conc. HCl: conc. HNO_3, volume ratio = 3 : 1).

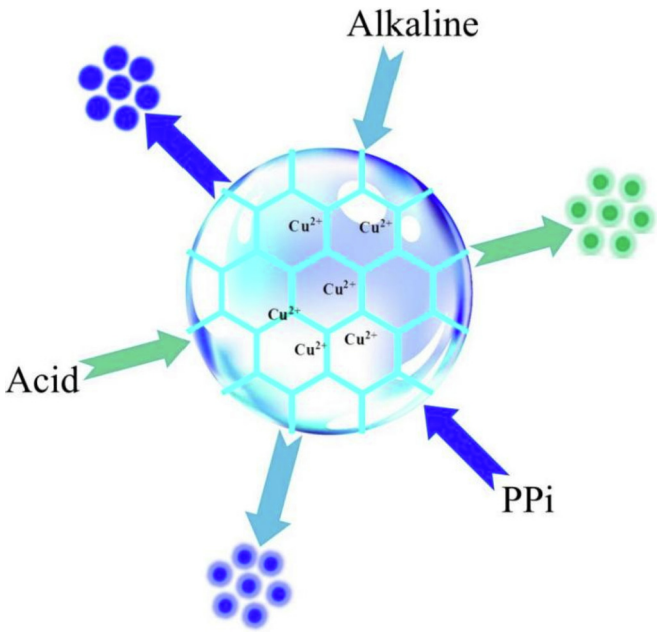

Scheme 1. Schematic diagram of pH and PPi sensing based on the multifunctional Cu-CDs.

2.2. Characterization

Fluorescence data were collected using FS5 Fluorescence Spectrophotometer. Transmission electron microscopy (TEM) images of the Cu-CDs were captured on a HT-7700 (Tokyo, Japan) with an accelerating voltage of 160 kV. High resolution TEM images were obtained by a FEI Tecnai F20 transmission electron microscope operating at an acceleration voltage of 200 kV. Ultraviolet–visible (UV–Vis) absorption spectra were measured by a U-2910 spectrophotometer (Hitachi, Japan). X-ray photoelectron spectroscopy (XPS) was performed on an ESCALAB 250XI electron spectrometer (Thermo, USA). Fluorescent photographs of the solution under UV light of 365 nm were operated with ZF-1 ultraviolet analyzer from Shanghai city Jihui scientific analyze instrument company. Fourier transform infrared (FTIR) spectrum data was recorded using a PerkinElmer FTIR spectrophotometer (PE-983, USA) using KBr pellet at room temperature. Fluorescence lifetime measurements were carried out on a FLS920 fluorescence spectrophotometer (Hitachi, Japan).

2.3. Green fabrication of the Cu-CDs.

The CDs were prepared by a one-step hydrothermal method. Typically, 0.3 g resorcinol, 0.15 g UR and 0.10 g $CuSO_4$ were added into 30 mL water. Ultrasonic irradiation of the mixture was conducted by an ultrasonic homogenizer until they were completely dissolved to homogeneous solution. Then the mixture was transferred to a Teflon-lined stainless-steel autoclave and heated at 180 ℃ for 7.0 h. After the autoclave was cooled down to room temperature naturally, the grayish yellow product was centrifuged for 20 min at 10000 rpm to remove large particles and then the supernatant was collected. Subsequently, the collected solution was dialyzed using a dialysis bag (1000 Da) for 10 h.

2.4. Fluorescence detection of PPi and pH in aqueous buffer

For the detection of PPi in solution, 100 μL of PPi with different concentrations were separately added into the mixture of 800 μL buffer solution (HEPES, 10 mM, pH = 6) containing the as-synthesized Cu-CDs (2.0 mg/mL). After 10 min, the fluorescence spectra were measured at the maximum excitation. The selectivity of the nanosensor toward PPi was evaluated by adding 100 μL of other anion solutions instead of PPi similarly. For the detection of pH, the prepared Cu-CDs were added into 800 μL of buffer solution with different pH (HEPES, 10 mM) and the fluorescence spectra were recorded in 15 min.

2.5. Procedure for the sewage samples

For the determination of PPi in real samples, the sewage was collected from the Huajin river in the campus of Anhui Normal University. The analysis of real samples was performed as follows: the sewage was pretreated by centrifugation at 10000 rpm for 10 min to get rid of the impurities after filtration. Then 0.22 μm membrane filter was used to remove the small particles. Finally, the sewage was diluted before using the real samples for measurements. In order to evaluate the accuracy of the proposed method, all the experiments were repeated three times to eliminate mutual interference.

2.6. Urine sample treatment

Human urine samples were obtained from laboratory staff. Morning urine was collected after 12 h of fasting overnight. Samples were immediately frozen and stored at −5 ℃ until analysis. Before the test, urine samples were thawed in a thermostatically controlled water bath at 37 ℃, and urine impurities were removed by centrifugation at 10000 rpm for 20 min to obtain urine supernatant. At the same time, a filter membrane was combined with centrifugation to eliminate the influence of salts and other impurities [39,40]. In this work, we focused on analyzing the urine supernatant, which mainly contains metabolites, and tried to eliminate any potential interfering signals caused by insoluble components in urine.

2.7. Naked-eye for urine pH on the test paper sensing

The filter paper was immersed into the Cu-CDs solution for 0.5 h. Then, the paper was removed from the solution and placed in an oven at 60 ℃ for 3 h until it was dried. The buffer solutions and urine samples with different pH (4, 5, 6, 7, 7.2, 7.5, 7.7 and 7.9) were dripped on filter paper. Then their fluorescence photographs were taken under UV light, respectively.

3. Results and discussion

3.1. Characterization of the Cu-CDs

The morphology and structure of the as-prepared Cu-CDs are shown in Fig. 1A and B, revealing that the Cu-CDs are well monodispersed in water, with an average particle size of approximately 2.55 nm. The high-resolution TEM (HRTEM) image of Cu-CDs shows well-resolved lattice fringes with an average in-plane lattice spacing of 0.21 nm (inset of Fig. 1), which are very close to the (100) diffraction facets of graphite [41]. The UV–vis absorption spectrum of the as-obtained Cu-CDs (Fig. 1C) display an evident absorption band at 276 nm [42], which is ascribed to the n-π^* transitions of C = O bonds transition of the Cu-CDs [43]. A strong fluorescence emission peak at 436 nm with a shoulder peak at 520 nm is observed at an optimal excitation wavelength of 370 nm (Fig. 1C). As illustrated in the inset of Fig. 1C, the obtained Cu-CDs show a bright blue light under the UV light (365 nm). The fluorescence emission peak of Cu-CDs at 436 nm (Fig. 1D) is excitation-independent with the excitation wavelength varying from 330 to 390 nm. This scenario may be due to the relative uniform surface states and size distribution[44,45].

In Fig. S1, the fluorescence decay of Cu-CDs monitored at 436 nm is in line with biexponential fitting curve with an average lifetime of 3.56 ns. Furthermore, an absolute fluorescence quantum yield (QY) of the Cu-CDs is determined by a widely used method [46], for which the QY of 8.51% in aqueous solution is calculated at 370 nm excitation. In order to investigate the optical characteristics of the Cu-CDs, the effect of time on stability is evaluated. Under the ultraviolet lamp for 90 min, the peak of fluorescence emission intensity is basically unchanged (Fig. S2), showing that the Cu-CDs are stable enough.

The functional groups of the surface of the Cu-CDs were studied by FTIR spectroscopy. As shown in Fig. 2A, the broad peak at about 3200–3500 cm^{-1} is assigned to the strong stretching vibration of O-H or N-H [47]. The absorption bands at 1356–1790 cm^{-1} are ascribed to the stretching vibrations of C-N , C-N – Cu, N – Cu – N and C = O [48,49]. The C = O vibration shifts to 1618 cm^{-1} while the peak at 1113 cm^{-1} indicates the presence of the C-O-C[50], suggesting that there are a lot of unsaturated carbon bonds formed during the carbonization process. The wide absorption peaks in the 400–650 regions are the spectra of inorganic compounds[51]. The absorption peak in the 617 cm^{-1} may correspond to the lattice vibrational modes of O-Cu [52,53].

Additionally, two peaks in the Raman spectrum (Fig. S3) of the Cu-CDs at 1322 cm^{-1} (D band) and 1589 cm^{-1} (G band) can be assigned to the areas of disorder or defects sp^3 and sp^2 carbon

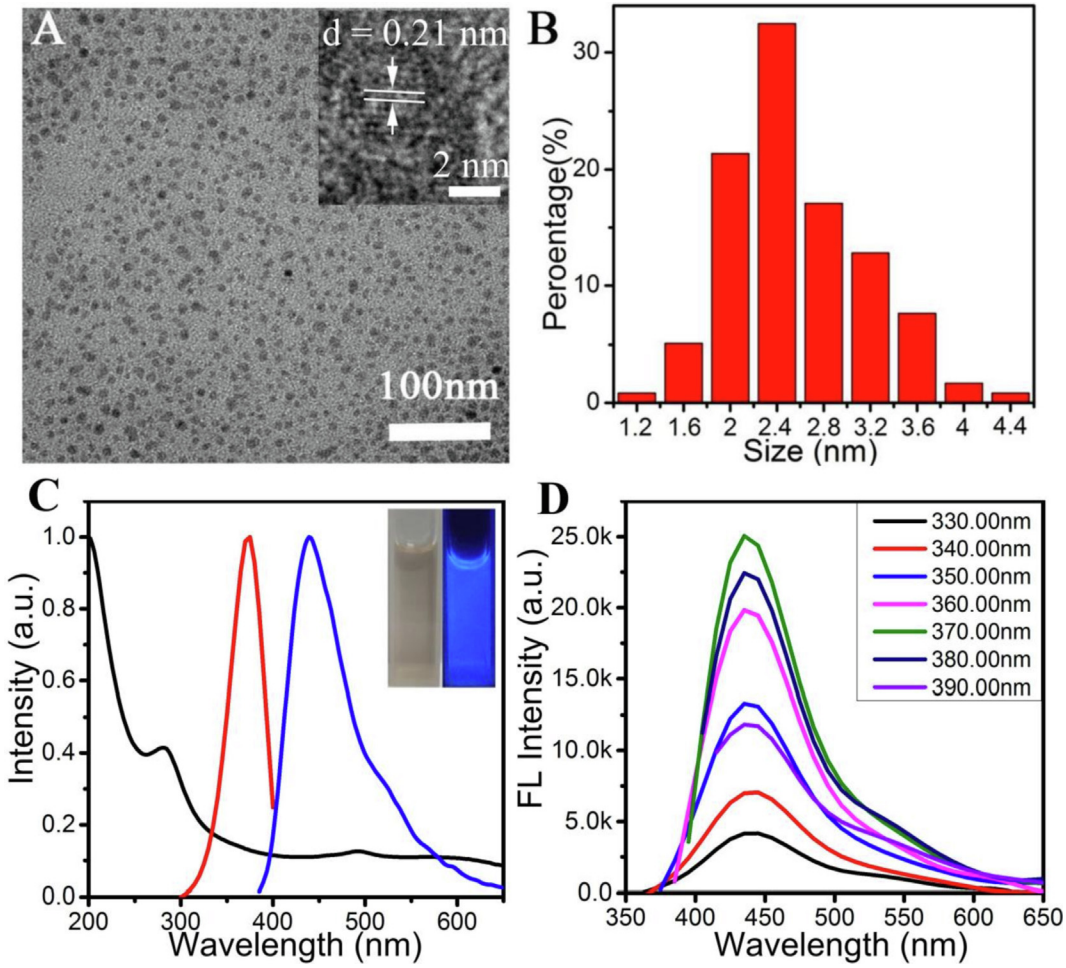

Fig. 1. (A) TEM image and (B) particle size distribution of the as-prepared Cu-CDs. (C) UV–vis absorption (black line), fluorescence excitation (red line) and fluorescence emission spectrum (blue line), respectively. Inset: the photographic images of the Cu-CDs under daylight (left) and UV light (right) at 365 nm excitation. (D) Fluorescence emission spectra of the Cu-CDs at the different excitation wavelengths.

atoms [54]. The intensity ratio of the D and G bands (I_D /I_G) is often used as an indicator of the defect degree in the structure of CDs [55]. Hereby, I_D / I_G = 0.47 reflects the existence of a large fraction of defects, which are mainly suffered from surface oxidation, in good agreement with the FTIR results.

XPS measurements were carried out to further identify the surface functional state and components of the Cu-CDs (Fig. 2 B-F). The full XPS spectrum of the Cu-CDs (Fig. 2B) present four typical peaks centered at 285.0 eV, 401.5 eV, 531.5 eV, and 935.0 eV, indicative of the existence of C (68.98 %), N (4.73 %), O (24.77 %) and Cu (1.52 %) elements in the Cu-CDs. As shown in Fig. 2C, the high-resolution C1s XPS spectrum consisted of three peaks locating at 288.2 eV, 284.4 eV, 285.8 eV are assigned to O-C/C = N, C = C/C-C and C-N, respectively. Meanwhile, N1s peaks at 399.9 eV and 401.4 eV (Fig. 2D) suggest that most of the N elements are in the form of N-H and amino N[56]. The peak at 399.3 eV (Fig. 2D) indicates the chelation of N to metal copper, which is also reflected in the FTIR (1500 and 1050 cm^{-1} bands)[57]. And the O1s peaks at binding energies of 533.0 eV and 531.9 eV can be ascribed to the O in the O-H, C-O-C and C = O groups (Fig. 2E). These peaks suggest that the Cu-CDs have logical hydrophilic properties as well as significant stability and dispersibility in water[58]. In addition, in Fig. 2F, the two peaks of Cu 2p3/2 and Cu 2p1/2 centered at 932.8 eV and 952.5 eV are assigned to Cu(I) species [59]. Observable satellite peaks (930–944 eV) are assigned to Cu(II) [60], which are the characteristic peaks of the divalent copper ion phase. The presence of a divalent copper ion imparts a great chelation ability for small molecules [61].

3.2. Sensing of the Cu-CDs towards PPi

We further evaluated the feasibility of Cu-CDs as a fluorescent sensing platform for PPi detection. We first demonstrated that the fluorescence intensity of Cu-CDs is almost unchanged under UV light (365 nm) for 90 min (Fig. S2), indicative of an excellent photo-stability of the Cu-CDs, which is a prerequisite for their application as a probe. While PPi is added to the Cu-CDs solution, the fluorescence of Cu-CDs is significantly enhanced (Fig. S4), suggesting the possibility of PPi sensing. To explore the optimal conditions for PPi sensing, the corresponding experiments were carried out. As shown in Fig S5, the optimal pH, carbonization temperature and dosage of the Cu-CDs, and incubation time are 6.0, 180 ℃, 2.0 mg/ mL and 10 min, respectively. To evaluate the selectivity of the Cu-CDs to PPi, the fluorescence responses of Cu-CDs to different ions were studied under the same conditions. The bars in Fig. 3A represent the fluorescence intensity ratio (F/F_0) of Cu-CDs (F_0: the fluorescence intensity of Cu-CDs, F: the fluorescence intensity of Cu-CDs with the addition of different ions). It can be observed that the fluorescence of Cu-CDs is enhanced significantly with the F/F_0 of 4.56 upon addition of PPi, whereas other ions have

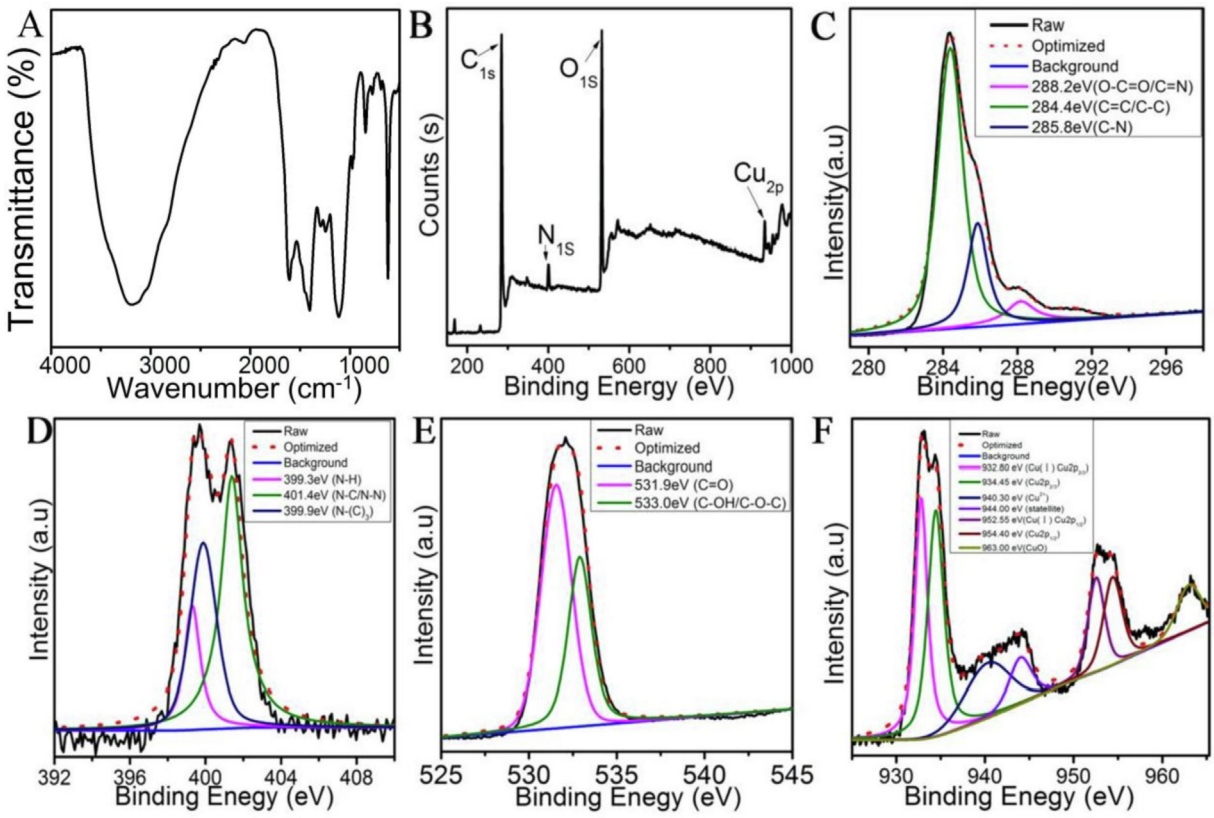

Fig. 2. (A) FTIR spectra of the Cu-CDs. (B) Full XPS spectra and (C-F) high-resolution XPS spectra of the Cu-CDs: (C) C1s, (D) N1s, (E) O1s, and (F) Cu2p.

negligible or no influence (F/F_0 between 0.80 and 1.61) on the fluorescence of Cu-CDs. These results suggest that the probe have a high selectivity towards PPi.

Under the optimized experimental conditions, we further investigated sensing capability of the Cu-CDs towards PPi. As described in Fig. 3B, the fluorescence intensity of the Cu-CDs at 436 nm gradually increases with the increase in concentration of PPi. In the range of 0.05–20 μM, a good linear relationship between the fluorescence intensity ratio ($(F - F_0)/F_0$) of the Cu-CDs and the concentration of PPi is presented (Fig. 3C). The linear fitting equation is $y = 0.1441x + 0.0340$ (x is the concentration of PPi, and y is $(F-F_0)/F_0$. Here, F_0 is the fluorescence intensity of Cu-CDs, F is the fluorescence intensity of Cu-CDs with the addition of PPi), $R^2 = 0.994$. The detection limit of PPi is 0.013 μM (3σ/slope, where σ was the relative standard deviation of blank solution), showing a remarkable sensitivity compared with previously reported methods (see Table S1). These results indicate that the proposed method provides a highly sensitive platform for the direct detection of PPi.

Then, we discussed the mechanism of why PPi enhances the fluorescence of the Cu-CDs. It was reported that the fluorescence of CDs can be enhanced through the surface passivation of organic species, polymer, or silica surface [62]. As PPi has a strong ability to bind metal ions, the enhancement in the fluorescence intensity can be anticipated by surface passivation [62,63]. To verify our expectation, the FTIR, fluorescence spectra, UV – vis absorption spectra, and zeta potential before and after the addition of PPi were measured. As shown in Fig. 3B, the fluorescence intensity of Cu-CDs at 436 nm can be greatly enhanced by the addition of PPi. As shown in Fig. 3D, the main infrared absorption peaks show no obvious difference. At the same time, as can be seen from Fig. S6, the UV–vis absorption spectrum of the solution at 200–450 nm increases with the addition of PPi, which provides a preliminary evidence that surface passivation has been presented [18,64]. Furthermore, the zeta potential of the prepared Cu-CDs is −8.19 mV, proving that carboxyl groups are in the majority. The presence of PPi initiates the increase of the zeta potential to −3.97 mV, which can be explained by the fact that PPi can partially shield the negatively charged carboxyl groups of Cu-CDs. This result further proves the occurrence of surface passivation[65,66].

3.3. Analysis of real samples

To evaluate the practical applicability of the Cu-CDs/PPi system, the standard addition method was employed to determine PPi in real sewage samples. As listed in Table 1, the recovery of PPi in these spiked samples is ranged from 97.90% to 102.20% with the relative standard deviation (RSD) within 3.74% (n = 3), indicating the practicability and reliability of the proposed sensing strategy.

3.4. Fluorescence response of the Cu-CDs toward pH

Then, the pH-sensitive behavior of the as-obtained Cu-CDs was investigated in 10 mM HEPES buffer with different pH values. As illustrated in Fig. 4A and Fig. 4B, under extremely acidic conditions (pH 3.0), the fluorescence is nearly completely quenched. It could be attributed to the protonation of carboxyl groups in the surface of Cu-CDs, resulting in aggregation of the Cu-CDs and the quenching of fluorescence [67–69]. In the subsequent observations, we found that the fluorescence intensity of Cu-CDs gradually increases with the increase of pH. Whereas, specifically, under alkaline conditions, the Cu-CDs emit strong blue fluorescence. A good linear relationship between the fluorescence intensity of Cu-CDs and pH from 6.0 to 8.7 was presented in Fig. 4C, the linear equation is $y = 34953.5x - 206020.06$ ($R^2 = 0.994$, x is the value of pH, and y is the value of fluorescence intensity of the Cu-CDs), which realizes the digital output for pH sensing. We then investigated

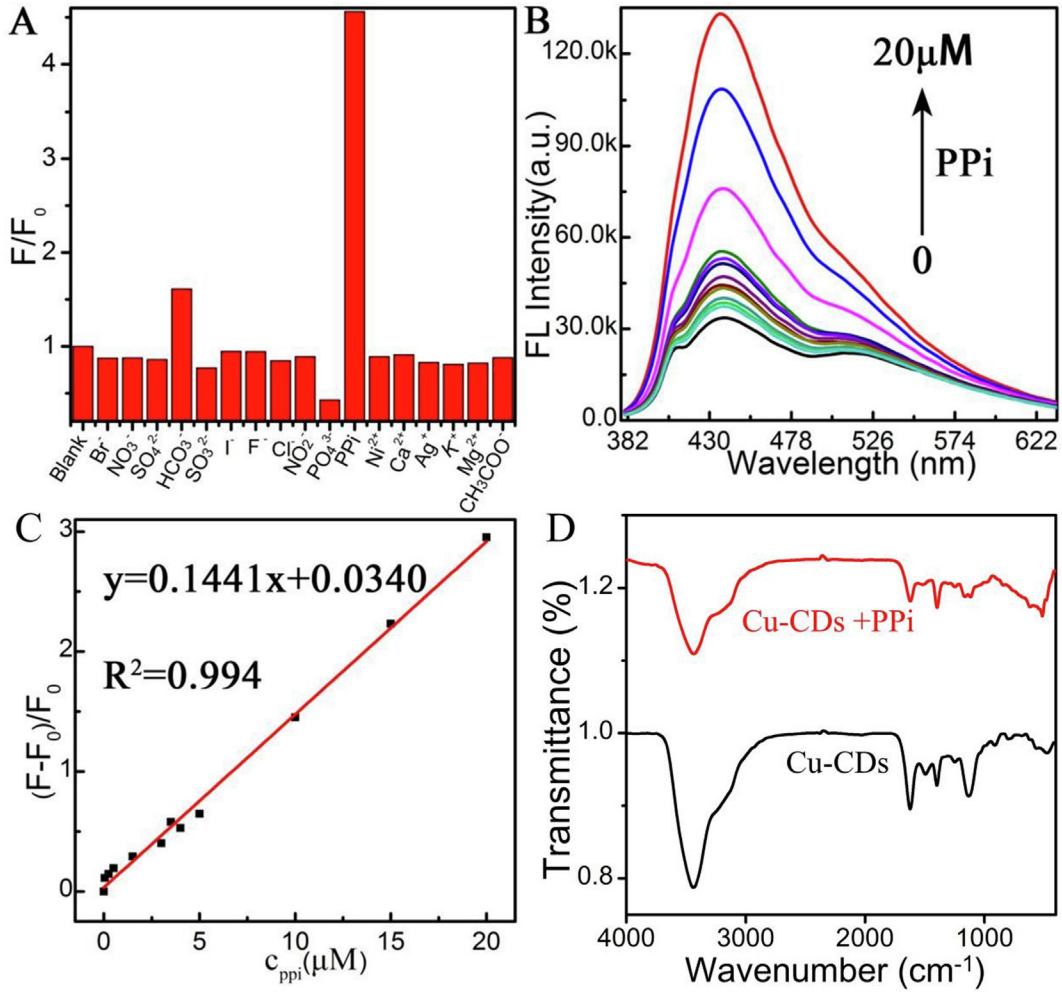

Fig. 3. (A) Selectivity of the Cu-CDs toward PPi (the concentration of all interfered anions were three times PPi). All experiments were carried out in HEPES buffer. (B) Fluorescence spectra of the Cu-CDs upon addition of different concentrations PPi under 370 nm excitation. (C) The linear relationship between $(F-F_0)/F_0$ and PPi concentration in the range of 0.05–20 μM. (D) The FTIR spectra of Cu-CDs in the absence and presence of PPi.

Table 1
Detection of PPi in real sewage samples.

Samples	Added /μM	Founded /μM	Recovery(n = 3, %)	RSD (%)
1	10	10.22	102.20	3.17
2	20	20.56	102.80	3.34
3	30	29.37	97.90	4.72

the accuracy of our developed method between the assay and the actual value. As can be seen in Table 2, the average relative standard deviation (RSD) is 1.72–4.42%. These findings suggest that the present method is both reliable and practical.

However, the luminescence mechanism of CDs is still an open question [65]. To investigate the mechanism of pH on the enhancement of fluorescence intensity of Cu-CDs, the UV/Vis absorption spectra and FTIR spectra of the Cu-CDs at different pH conditions were measured. As can be seen from Fig. S7, the characteristic peak intensity of the UV–vis absorption spectrum at 200–450 nm increases with the increase of pH value, and there is no shift in the position of the peak. For comparison, the FTIR spectrum under different pH conditions of Cu-CDs were recorded (Fig. 4D). It was found that there is no significant difference. By analogy with the Cu-CDs/PPi system, we found that the principle of fluorescence intensity enhancement of Cu-CDs with pH value may also be due to the surface passivation effect [62,64].

To investigate the photostability of the Cu-CDs, time scans of the fluorescence intensity in 10 mM HEPES buffer with different pH values (5.0, 7.0 and 8.8) were carried out for 60 min. It was demonstrated that the fluorescence intensity remains stable during the scanning process (Fig. S8), indicative of their photostabilities under light and air at the certain pH value. Therefore, the as-synthesized Cu-CDs could be applied as a new kind of nanoprobes for pH sensing.

Correspondingly, a gradient color change under UV light (365 nm) can be observed along with the pH changes. As shown in Fig. 4E, under acidic conditions, the solution with green fluorescence is observed. With the increase in pH value, the green fluorescence brightness gets significantly brighter. At variance, under neutral and alkaline conditions, the green fluorescence is changed to blue fluorescence, and then the fluorescence brightness increases gradually with the increase of pH. These variation means that visual detection of pH by naked eyes would be realized for the

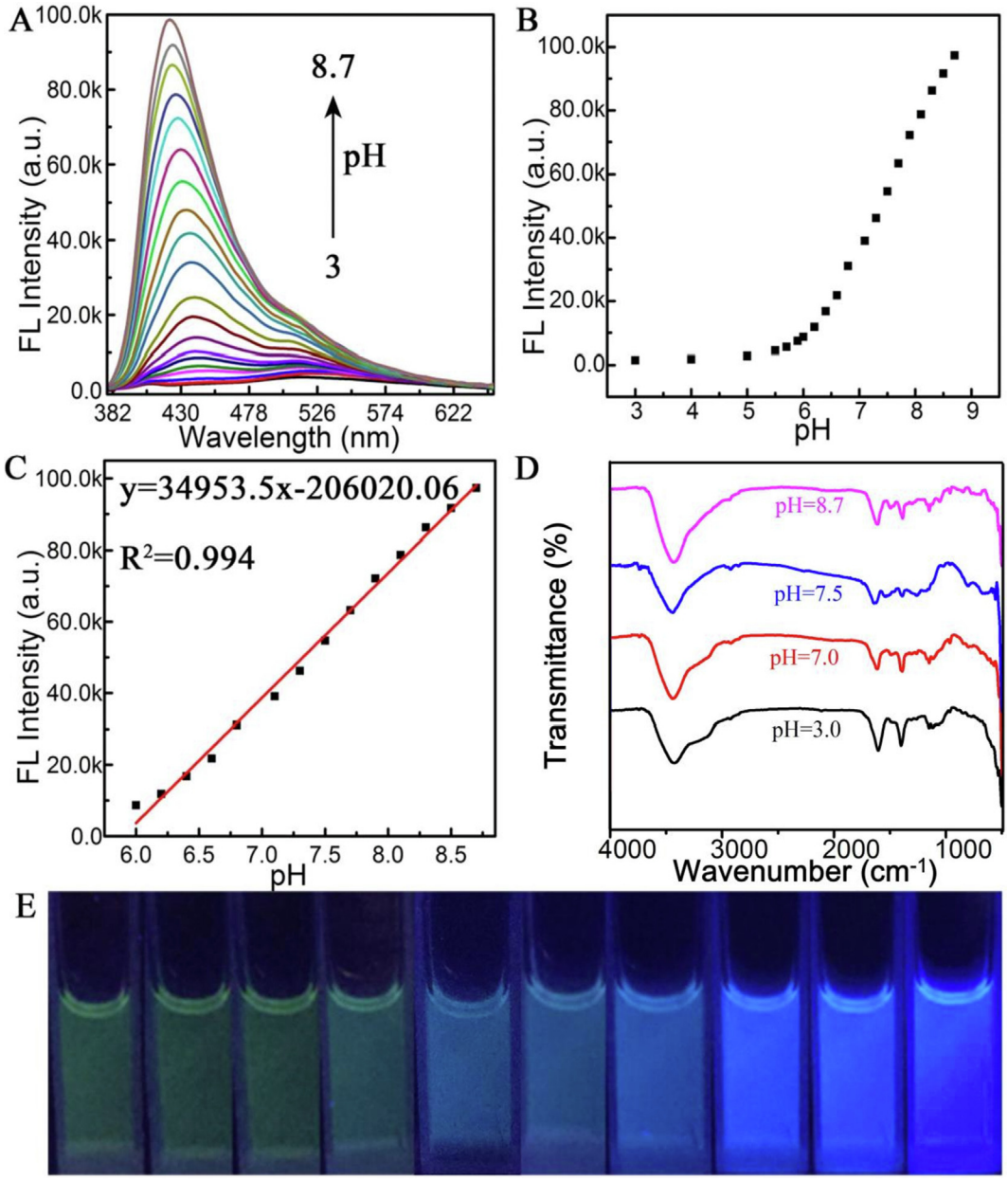

Fig. 4. (A) Fluorescence spectra of the Cu-CDs dispersed in the solutions with different pH values (from 3 to 8.7). (B) FL intensity at the peak position of the Cu-CDs dispersed in the solutions with different pH values. (C) Linear relationship between FL intensity and pH in the range of 6.0–8.7 and (D) The FTIR spectra of Cu-CDs in different pH buffers. (E) The corresponding solution of the synthesized Cu-CDs in different pH buffer solutions under ultraviolet light irradiation: pH = 3–8.7 (from left to right).

Table 2
pH comparison between the measured value and the actual value.

Samples	Actual pH	Measured pH	Recovery (n = 3, %)	RSD (%)
1	3.0	2.88	96.00	3.45
2	7.0	7.11	101.58	1.72
3	7.5	7.34	97.87	2.13
4	8.7	8.86	102.28	4.42

promising applicability for biosensing in the future [70,71]. In Fig. 4A, the characteristic peak of the Cu-CDs is at 436 nm with a shoulder peak at 520 nm. No obvious change in the characteristic peak position, only the change in intensity is observed with the change in pH value [72,73]. Thus, the color change is more likely to be triggered by mixing the blue color at 436 nm with the green color at 520 nm [74,75]. Note that the fluorescence intensity at 436 nm is particularly sensitive to the pH value. However, the shoulder peak at 520 nm does not change much when the pH conditions are changed. Overall, in the strongly acidic case, both peaks are involved in the presence of green color. With the increase of pH, the blue color at 436 nm gradually becomes dominated, leading to the transition phenomenon from final green to blue color [76,77].

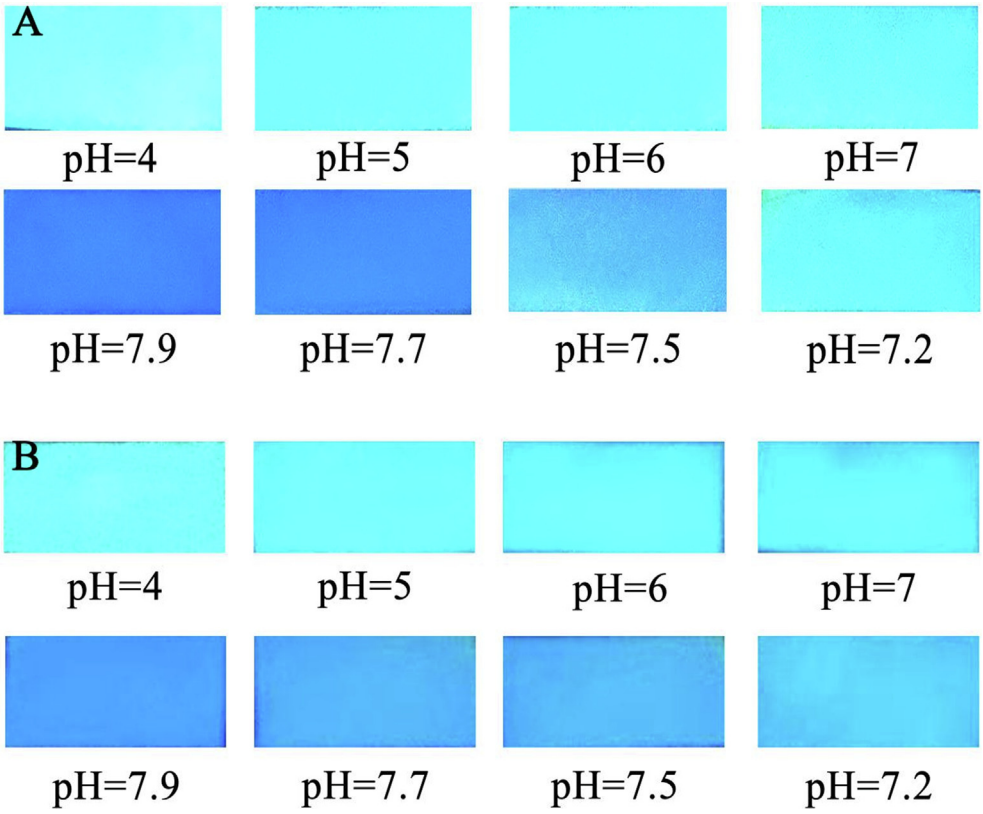

Fig. 5. (A) The photographs of filter paper coated with the Cu-CDs (pH = 4, 5, 6, 7, 7.2, 7.5, 7.7, 7.9). (B) The photographs of filter paper coated with the Cu-CDs after dripping urine of different pH (4, 5, 6, 7, 7.2, 7.5, 7.7, 7.9).

3.5. Naked-eye visualization for urine pH

We further used the Cu-CDs cross-linked in commercial cellulose filter paper to prepare the pH strip and realize the naked-eye fluorescence detection of pH. Under UV light radiation, the Cu-CDs papers exhibit bright fluorescence (Fig. 5), while the untreated paper is nonluminous, demonstrating the successful preparation of Cu-CDs coated paper [73]. The buffer solutions with pH values of 4, 5, 6, 7, 7.2, 7.5, 7.7 and 7.9 were dripped on eight pieces of fluorescent paper and dried for 3 h, the corresponding photographs under UV-lamp are shown in Fig. 5A. Under acidic conditions of pH = 4 and 5, the strips show green fluorescence which can be visualized by the naked eye, and the color changes from green to blue in the pH range of 6–7.5. When pH reaches 7.7, the distinct blue on the Cu-CDs coated papers is observed. The change of colors is consistent with that in an aqueous solution. Then, the paper-based Cu-CDs fluorescent sensing platform was applied to urine pH assay. Similar to the above results, the color of filter paper coated with the Cu-CDs shows a trend of changing with the increase of urine pH from 4 to 7.9 (Fig. 5B). These results demonstrate that the proposed Cu-CDs-based paper is capable of monitoring small fluctuations of pH in real urine samples by naked eye. In comparison with other pH-sensitive nanocomposites-based sensors[16], our proposed pH sensor has a more sensitive discoloration point, which is more sensitive to the small environmental change in body fluids.

4. Conclusion

In conclusion, we have successfully synthesized fluorescent Cu-CDs by hydrothermal method with resorcinol, UR and $CuSO_4$ as the precursors. The as-obtained Cu-CDs can be served as fluorescent nanoprobes to detect PPi with high sensitivity and selectivity. The LOD was calculated to be 0.013 μM with linearity from 0.05 to 20 μM. The Cu-CDs presented a pH-dependent fluorescence emission feature, and the fluorescence intensity of the Cu-CDs was enhanced along with the increase of pH and had a good linear relationship against pH values from 6 to 8.7 in HEPES buffer solution. Further, a fluorescent paper coated with the Cu-CDs for visual detection of pH by naked eyes has been successfully prepared, and the Cu-CDs-based paper were applied to monitor urine pH with a good satisfaction. We believe that on one hand, the Cu-CDs have a great prospect in the detection of PPi, and on the other hand, the constructed easy-to-use nanoprobe-based paper would offer the promising insights for developing the portable pH sensor.

CRediT authorship contribution statement

Ying Yang: Data curation, Writing – original draft. **Chaofeng Wang:** Data curation, Writing – original draft. **Qin Shu:** Investigation. **Na Xu:** Investigation. **Shuangqing Qi:** Formal analysis. **Shujuan Zhuo:** Investigation, Methodology, Supervision. **Changqing Zhu:** Resources. **Jinyan Du:** Investigation, Methodology, Project administration, Resources, Supervision, Writing – review & editing.

Declaration of Competing Interest

The authors declare that they have no known competing financial interests or personal relationships that could have appeared to influence the work reported in this paper.

Acknowledgments

This work was financially supported by the National Natural Science Foundation of China (No. 21705003).

Appendix A. Supplementary data

Supplementary data to this article can be found online at https://doi.org/10.1016/j.saa.2021.120681.

References

[1] B.K. Datta, D. Thiyagarajan, S. Samanta, A. Ramesh, G. Das, A novel chemosensor with visible light excitability for sensing Zn^{2+} in physiological medium and in HeLa cells, Org Biomol Chem 12 (2014) 4975–4982.

[2] H.T. Ngo, X. Liu, K.A. Jolliffe, Anion recognition and sensing with Zn(II)-dipicolylamine complexes, Chem Soc Rev 41 (2012) 4928–4965.

[3] L.M. Mesquita, V. Andre, C.V. Esteves, T. Palmeira, M.N. Berberan-Santos, P. Mateus, R. Delgado, Dinuclear Zinc(II) Macrocyclic Complex as Receptor for Selective Fluorescence Sensing of Pyrophosphate, Inorg Chem 55 (2016) 2212–2219.

[4] X. Feng, Y. An, Z. Yao, C. Li, G. Shi, A turn-on fluorescent sensor for pyrophosphate based on the disassembly of Cu^{2+}-mediated perylene diimide aggregates, ACS Appl Mater Interfaces 4 (2012) 614–618.

[5] D. Chao, Y. Zhang, Anion-induced emissive nanoparticles for tunable fluorescence detection of pyrophosphate and bioimaging application, Sen. Actuators B 242 (2017) 253–259.

[6] J. Wang, X. Liu, Y. Pang, A Benzothiazole-Based Sensor for Pyrophosphate (PPi) and ATP: Mechanistic Insight for Anion-Induced ESIPT Turn-On, J. Mater. Chem. B. 2 (2014) 6634–6638.

[7] V.E. Zwicker, B.M. Long, K.A. Jolliffe, Selective sensing of pyrophosphate in physiological media using zinc(II)dipicolylamino-functionalised peptides, Org Biomol Chem 13 (2015) 7822–7829.

[8] Y.W. Wang, S.B. Liu, Y.L. Yang, P.Z. Wang, A.J. Zhang, Y. Peng, A terbium(III)-complex-based on-off fluorescent chemosensor for phosphate anions in aqueous solution and its application in molecular logic gates, ACS Appl Mater Interfaces 7 (2015) 4415–4422.

[9] X. An, Q. Tan, S. Pan, H. Liu, X. Hu, A turn-on luminescence probe based on amino-functionalized metal-organic frameworks for the selective detections of Cu(2+), Pb(2+) and pyrophosphate, Spectrochim. Acta, Part A 247 (2021) 119073.

[10] T. Wang, Q. Pang, Z. Tong, M. Wang, N. Xiao, Selective sensing of PPi by fluorogenic Al(III)-probe complex in aqueous medium, Spectrochim. Acta, Part A 250 (2021) 119249.

[11] S. Zhang, X. Ji, J. Liu, Q. Wang, L. Jin, One-step synthesis of yellow-emissive carbon dots with a large Stokes shift and their application in fluorimetric imaging of intracellular pH, Spectrochim. Acta, Part A 227 (2020) 117677.

[12] W.L. Shelver, D.J. Smith, L.A. Tell, R.E. Baynes, J.W. Schroeder, J.E. Riviere, Screening and Confirmatory Analyses of Flunixin in Tissues and Bodily Fluids after Intravenous or Intramuscular Administration to Cull Dairy Cows with or without Lipopolysaccharide Challenge, J Agric Food Chem 64 (2016) 336–345.

[13] R.D. Espy, S.F. Teunissen, N.E. Manicke, Y. Ren, Z. Ouyang, A. van Asten, R.G. Cooks, Paper spray and extraction spray mass spectrometry for the direct and simultaneous quantification of eight drugs of abuse in whole blood, Anal Chem 86 (2014) 7712–7718.

[14] N.D. Chubatyi, C.N. McEwen, Improving the Sensitivity of Matrix-Assisted Ionization (MAI) Mass Spectrometry Using Ammonium Salts, J Am Soc Mass Spectrom 26 (2015) 1649–1656.

[15] T. Fukuda, L. Ewan, M. Bauer, R.J. Mattaliano, K. Zaal, E. Ralston, P.H. Plotz, N. Raben, Dysfunction of endocytic and autophagic pathways in a lysosomal storage disease, Ann Neurol 59 (2006) 700–708.

[16] J. Shangguan, D. He, X. He, K. Wang, F. Xu, J. Liu, J. Tang, X. Yang, J. Huang, Label-Free Carbon-Dots-Based Ratiometric Fluorescence pH Nanoprobes for Intracellular pH Sensing, Anal Chem 88 (2016) 7837–7843.

[17] K. Hola, A.B. Bourlinos, O. Kozak, K. Berka, K.M. Siskova, M. Havrdova, J. Tucek, K. Safarova, M. Otyepka, E.P. Giannelis, R. Zboril, Photoluminescence effects of graphitic core size and surface functional groups in carbon dots: COO^{-} induced red-shift emission, Carbon 70 (2014) 279–286.

[18] Z.A. Qiao, Y. Wang, Y. Gao, H. Li, T. Dai, Y. Liu, Q. Huo, Commercially activated carbon as the source for producing multicolor photoluminescent carbon dots by chemical oxidation, Chem Commun (Camb) 46 (2010) 8812–8814.

[19] T. Li, J. Cao, Z. Li, X. Wang, P. He, Broad screening and identification of beta-agonists in feed and animal body fluid and tissues using ultra-high performance liquid chromatography-quadrupole-orbitrap high resolution mass spectrometry combined with spectra library search, Food Chem 192 (2016) 188–196.

[20] Y.P. Lin, Y.L. Lee, C.Y. Hung, W.J. Huang, S.C. Lin, Determination of multiresidue analysis of beta-agonists in muscle and viscera using liquid chromatograph/tandem mass spectrometry with Quick, Easy, Cheap, Effective, Rugged, and Safe methodologies, J Food Drug Anal 25 (2017) 275–284.

[21] L. Gan, Q. Su, Z. Chen, X. Yang, Exploration of pH-responsive carbon dots for detecting nitrite and ascorbic acid, Applied Surface Science 530 (2020) 147269.

[22] J. Bai, Y. Ma, G. Yuan, X. Chen, J. Mei, L. Zhang, L. Ren, Solvent-controlled and solvent-dependent strategies for the synthesis of multicolor carbon dots for pH sensing and cell imaging, J. Mater. Chem. C 7 (2019) 9709–9718.

[23] S. Hu, X. Meng, F. Tian, W. Yang, N. Li, C. Xue, J. Yang, Q. Chang, Dual photoluminescence centers from inorganic-salt-functionalized carbon dots for ratiometric pH sensing, J. Mater. Chem. C 5 (2017) 9849–9853.

[24] C. Xia, M. Cao, J. Xia, G. Zhou, D. Jiang, D. Zhang, J. Wang, H. Li, An ultrafast responsive and sensitive ratiometric fluorescent pH nanoprobe based on label-free dual-emission carbon dots, J. Mater. Chem. C 7 (2019) 2563–2569.

[25] J. Huang, K. Pu, Activatable Molecular Probes for Second Near-Infrared Fluorescence, Chemiluminescence, and Photoacoustic Imaging, Angew Chem Int Ed Engl 59 (2020) 11717–11731.

[26] Y. Fang, J. Shang, D. Liu, W. Shi, X. Li, H. Ma, Design, Synthesis, and Application of a Small Molecular NIR-II Fluorophore with Maximal Emission beyond 1200 nm, J Am Chem Soc 142 (2020) 15271–15275.

[27] L. Wu, L. Chen, M. Kou, Y. Dong, W. Deng, L. Ge, H. Bao, Q. Chen, D. Li, The ratiometric fluorescent probes for monitoring the reactive inorganic sulfur species (RISS) signal in the living cell, Spectrochim. Acta, Part A 231 (2020) 118141.

[28] K.K. Chan, S.H.K. Yap, K.T. Yong, Biogreen Synthesis of Carbon Dots for Biotechnology and Nanomedicine Applications, Nanomicro Lett 10 (2018) 72.

[29] S. Chen, T. Sun, M. Zheng, Z. Xie, Carbon Dots Based Nanoscale Covalent Organic Frameworks for Photodynamic Therapy, Adv Funct Mater 30 (2020) 2004680.

[30] X. Xu, D. Ren, Y. Chai, X. Cheng, J. Mei, J. Bao, F. Wei, G. Xu, Q. Hu, Y. Cen, Dual-emission carbon dots-based fluorescent probe for ratiometric sensing of Fe(III) and pyrophosphate in biological samples, Sensors Actuators, B 298 (2019) 126829.

[31] Q. Yue, Y. Hou, S. Yue, K. Du, T. Shen, L. Wang, S. Xu, H. Li, J. Liu, Construction of an off-on fluorescence system based on carbon dots for trace pyrophosphate sensing, J Fluoresc 25 (2015) 585–594.

[32] Y. Hu, X. Geng, L. Zhang, Z. Huang, J. Ge, Z. Li, Nitrogen-doped Carbon Dots Mediated Fluorescent on-off Assay for Rapid and Highly Sensitive Pyrophosphate and Alkaline Phosphatase Detection, Sci Rep 7 (2017) 5849.

[33] A. Yu, Y. Tang, K. Li, J. Gao, Y. Zheng, Z. Zeng, Tunable photoluminescence studies based on blue-emissive carbon dots and sequential determination of Fe(III) and pyrophosphate ions, Spectrochim. Acta, Part A 222 (2019) 117231.

[34] Y. Dai, Z. Liu, Y. Bai, Z. Chen, J. Qin, F. Feng, A novel highly fluorescent S, N, O co-doped carbon dots for biosensing and bioimaging of copper ions in live cells, RSC Adv 8 (2018) 42246–42252.

[35] Y. Liu, Q. Zhou, Y. Yuan, Y. Wu, Hydrothermal synthesis of fluorescent carbon dots from sodium citrate and polyacrylamide and their highly selective detection of lead and pyrophosphate, Carbon 115 (2017) 550–560.

[36] J. Wang, X. Wang, X. Pan, W. Pan, Y. Li, X. Liang, X. Sun, Dual-emission carbon dots achieved by luminescence center modulation within one-pot synthesis for a fluorescent ratiometric probe of pH, Hg(2+), and glutathione, Mikrochim Acta 187 (2020) 330.

[37] H. Nie, M. Li, Q. Li, S. Liang, Y. Tan, L. Sheng, W. Shi, S.-X.-A. Zhang, Carbon Dots with Continuously Tunable Full-Color Emission and Their Application in Ratiometric pH Sensing, Chem Mater 26 (2014) 3104–3112.

[38] M. Zhang, R. Su, J. Zhong, L. Fei, W. Cai, Q. Guan, W. Li, N. Li, Y. Chen, L. Cai, Q. Xu, Red/orange dual-emissive carbon dots for pH sensing and cell imaging, J. Nano Res 12 (2019) 815–821.

[39] J. Huang, Y. He, Z. Zhang, B. Lei, W. Wu, Synthesis of high-efficient red carbon dots for pH detection, J Lumin 215 (2019) 116640.

[40] Y. Hu, Z. Gao, J. Yang, H. Chen, L. Han, Environmentally benign conversion of waste polyethylene terephthalate to fluorescent carbon dots for "on-off-on" sensing of ferric and pyrophosphate ions, J Colloid Interface Sci 538 (2019) 481–488.

[41] R. Atchudan, T.N.J.I. Edison, S. Perumal, N. Muthuchamy, Y.R. Lee, Hydrophilic nitrogen-doped carbon dots from biowaste using dwarf banana peel for environmental and biological applications, Fuel 275 (2020) 117821.

[42] H. Wu, Y. Yan, Q. Huang, G. Liang, F. Qiu, Z. Ye, D. Liu, A simple, cost-effective and selective analysis of glucose via electrochemical impedance sensing based on copper and nitrogen co-doped carbon quantum dots, New J. Chem 44 (2020) 12723–12728.

[43] M. Zheng, Z. Xie, D. Qu, D. Li, P. Du, X. Jing, Z. Sun, On-off-on fluorescent carbon dot nanosensor for recognition of chromium(VI) and ascorbic acid based on the inner filter effect, ACS Appl Mater Interfaces 5 (2013) 13242–13247.

[44] H. Peng, Y. Li, C. Jiang, C. Luo, R. Qi, R. Huang, C.-G. Duan, J. Travas-Sejdic, Tuning the properties of luminescent nitrogen-doped carbon dots by reaction precursors, Carbon 100 (2016) 386–394.

[45] Y. Liu, W. Duan, W. Song, J. Liu, C. Ren, J. Wu, D. Liu, H. Chen, Red Emission B, N, S-co-Doped Carbon Dots for Colorimetric and Fluorescent Dual Mode Detection of Fe(3+) Ions in Complex Biological Fluids and Living Cells, ACS Appl Mater Interfaces 9 (2017) 12663–12672.

[46] S. Huang, E. Yang, J. Yao, Y. Liu, Q. Xiao, Red emission nitrogen, boron, sulfur co-doped carbon dots for "on-off-on" fluorescent mode detection of Ag(+) ions and l-cysteine in complex biological fluids and living cells, Anal Chim Acta 1035 (2018) 192–202.

[47] B. Wu, X. Liu, X. Shi, W. Han, C. Wang, L. Jiang, Highly photoluminescent and temperature-sensitive P, N, B-co-doped carbon quantum dots and their highly sensitive recognition for curcumin, RSC Adv 9 (2019) 8340–8349.

[48] W. Lu, X. Gong, M. Nan, Y. Liu, S. Shuang, C. Dong, Comparative study for N and S doped carbon dots: Synthesis, characterization and applications for Fe(3+) probe and cellular imaging, Anal Chim Acta 898 (2015) 116–127.

[49] Z.X. Liu, B.B. Chen, M.L. Liu, H.Y. Zou, C.Z. Huang, Cu(i)-Doped carbon quantum dots with zigzag edge structures for highly efficient catalysis of azide–alkyne cycloadditions, Green Chem 19 (2017) 1494–1498.

[50] J. Ju, R. Zhang, S. He, W. Chen, Nitrogen-doped graphene quantum dots-based fluorescent probe for the sensitive turn-on detection of glutathione and its cellular imaging, RSC Adv. 4 (2014) 52583–52589.
[51] Q. Wang, S. Zhang, Y. Zhong, X.F. Yang, Z. Li, H. Li, Preparation of Yellow-Green-Emissive Carbon Dots and Their Application in Constructing a Fluorescent Turn-On Nanoprobe for Imaging of Selenol in Living Cells, Anal Chem 89 (2017) 1734–1741.
[52] B. Jia, Y. Zhao, Z. Zhang, L. Liu, M. Qin, H. Wu, Y. Liu, X. Qu, G. Qi, Borax promotes the facile formation of hollow structure in Cu single crystalline nanoparticles for multifunctional electrocatalysis, Inorg Chem Front 6 (2019) 893–902.
[53] N. Rahemi, M. Haghighi, A.A. Babaluo, M.F. Jafari, S. Khorram, Non-thermal plasma assisted synthesis and physicochemical characterizations of Co and Cu doped Ni/Al2O3 nanocatalysts used for dry reforming of methane, Int J. Hydr. ogen, Energy 38 (2013) 16048–16061.
[54] J. Zhao, F. Li, S. Zhang, Y. An, S. Sun, Preparation of N-doped yellow carbon dots and N, P co-doped red carbon dots for bioimaging and photodynamic therapy of tumors, New J. Chem 43 (2019) 6332–6342.
[55] Y. Fu, S. Zhao, S. Wu, L. Huang, T. Xu, X. Xing, M. Lan, X. Song, A carbon dots-based fluorescent probe for turn-on sensing of ampicillin, Dyes Pigm 172 (2020) 107846.
[56] L. Song, Y. Cui, C. Zhang, Z. Hu, X. Liu, Microwave-assisted facile synthesis of yellow fluorescent carbon dots from o-phenylenediamine for cell imaging and sensitive detection of Fe^{3+} and H_2O_2, RSC Adv 6 (2016) 17704–17712.
[57] P.P. Zhu, Z. Cheng, L.L. Du, Q. Chen, K.J. Tan, Synthesis of the Cu-Doped Dual-Emission Fluorescent Carbon Dots and Its Analytical Application, Langmuir 34 (2018) 9982–9989.
[58] R. Wang, X. Wang, Y. Sun, One-step synthesis of self-doped carbon dots with highly photoluminescence as multifunctional biosensors for detection of iron ions and pH, Sens Actuators B 241 (2017) 73–79.
[59] P. Cao, K. Zhao, X. Quan, S. Chen, H. Yu, Efficient and stable heterogeneous electro-Fenton system using iron oxides embedded in Cu, N co-doped hollow porous carbon as functional electrocatalyst, Sep Purif Technol 238 (2020) 116424.
[60] P. Liu, E.J. Hensen, Highly efficient and robust Au/$MgCuCr_2O_4$ catalyst for gas-phase oxidation of ethanol to acetaldehyde, J Am Chem Soc 135 (2013) 14032–14035.
[61] J. Du, Y. Yang, T. Shao, S. Qi, P. Zhang, S. Zhuo, C. Zhu, Yellow emission carbon dots for highly selective and sensitive OFF-ON sensing of ferric and pyrophosphate ions in living cells, J Colloid Interface Sci 587 (2021) 376–384.
[62] W. Song, W. Duan, Y. Liu, Z. Ye, Y. Chen, H. Chen, S. Qi, J. Wu, D. Liu, L. Xiao, C. Ren, X. Chen, Ratiometric Detection of Intracellular Lysine and pH with One-Pot Synthesized Dual Emissive Carbon Dots, Anal Chem 89 (2017) 13626–13633.
[63] B. Zhu, S. Sun, Y. Wang, S. Deng, G. Qian, M. Wang, A. Hu, Preparation of carbon nanodots from single chain polymeric nanoparticles and theoretical investigation of the photoluminescence mechanism, J. Mater. Chem. C 1 (2013) 580–586.
[64] H. Li, Z. Kang, Y. Liu, S.-T. Lee, Carbon nanodots: synthesis, properties and applications, J. Mater. Chem. 22 (46) (2012) 24230.
[65] L. Li, G. Wu, G. Yang, J. Peng, J. Zhao, J.J. Zhu, Focusing on luminescent graphene quantum dots: current status and future perspectives, Nanoscale 5 (2013) 4015–4039.
[66] P. Yang, J. Zhao, L. Zhang, L. Li, Z. Zhu, Intramolecular Hydrogen Bonds Quench Photoluminescence and Enhance Photocatalytic Activity of Carbon Nanodots, Chem - Eur J 21 (2015) 8561–8568.
[67] D. Zhong, H. Miao, K. Yang, X. Yang, Carbon dots originated from carnation for fluorescent and colorimetric pH sensing, Mater Lett 166 (2016) 89–92.
[68] H. Zhang, M. Tian, R. Yang, X. He, X. Yu, A general strategy to increase emission shift of two-photon ratiometric pH probes using a reversible intramolecular reaction of spiro-oxazolidine, Spectrochim. Acta, Part A 246 (2021) 119035.
[69] M.A. Treto-Suárez, Y. Hidalgo-Rosa, E. Schott, D. Páez-Hernández, X. Zarate, Fluorescence turn-on and turn-off mechanisms of a dual-selective chemosensor of Bi^{3+} and pH changes: Insights from a theoretical perspective, Dyes Pigm 185 (2021) 108934.
[70] Y. Yan, H. Yu, K. Zhang, M. Sun, Y. Zhang, X. Wang, S. Wang, Dual-emissive nanohybrid of carbon dots and gold nanoclusters for sensitive determination of mercuric ions, J. Nano Res 9 (2016) 2088–2096.
[71] C. Zou, M.F. Foda, X. Tan, K. Shao, L. Wu, Z. Lu, H.S. Bahlol, H. Han, Carbon-Dot and Quantum-Dot-Coated Dual-Emission Core-Satellite Silica Nanoparticles for Ratiometric Intracellular Cu(2+) Imaging, Anal Chem 88 (2016) 7395–7403.
[72] C. Wang, H. Lin, Z. Xu, Y. Huang, M.G. Humphrey, C. Zhang, Tunable Carbon-Dot-Based Dual-Emission Fluorescent Nanohybrids for Ratiometric Optical Thermometry in Living Cells, ACS Appl Mater Interfaces 8 (2016) 6621–6628.
[73] C. Wang, T. Hu, T. Thomas, S. Song, Z. Wen, C. Wang, Q. Song, M. Yang, Surface state-controlled C-dot/C-dot based dual-emission fluorescent nanothermometers for intra-cellular thermometry, Nanoscale 10 (2018) 21809–21817.
[74] A. Zhu, Q. Qu, X. Shao, B. Kong, Y. Tian, Carbon-dot-based dual-emission nanohybrid produces a ratiometric fluorescent sensor for in vivo imaging of cellular copper ions, Angew Chem Int Ed Engl 51 (2012) 7185–7189.
[75] T.K. Mondal, U.K. Ghorai, S.K. Saha, Dual-Emissive Carbon Quantum Dot-Tb Nanocomposite as a Fluorescent Indicator for a Highly Selective Visual Detection of Hg(II) in Water, ACS Omega 3 (2018) 11439–11446.
[76] A. Pal, K. Ahmad, D. Dutta, A. Chattopadhyay, Boron Doped Carbon Dots with Unusually High Photoluminescence Quantum Yield for Ratiometric Intracellular pH Sensing, Chemphyschem 20 (2019) 1018–1027.
[77] P. Zhu, J. Li, L. Gao, J. Xiong, K. Tan, Strategy to Synthesize Tunable Multiemission Carbon Dots and Their Multicolor Visualization Application, ACS Appl Mater Interfaces 13 (2021) 33354–33362.